

# Quantitative Nanometer-scale X-ray Phase Tomography

P. J. McMahon,<sup>1</sup> A. G. Peele,<sup>1</sup> D. Paterson,<sup>2</sup> J. Lin,<sup>1</sup> T. H. K. Irving,<sup>1</sup> I. McNulty,<sup>2</sup> K. A. Nugent<sup>1</sup>

<sup>1</sup>School of Physics, University of Melbourne, Victoria, Australia

<sup>2</sup>Advanced Photon Source, Argonne National Laboratory, Argonne, IL, U.S.A.

## Introduction

In recent years, there have been many advances in the field of x-ray imaging. These may be attributed to improvements in charged-coupled device (CCD) detectors and optical components, but the main driving force is the significant increase in flux and coherence obtained from using third-generation synchrotrons such as the APS.

A notable example is the growth in x-ray phase imaging, where information on the structure and composition of an object is obtained from the refractive interaction of x-rays with matter. This can be compared with more traditional techniques based on absorption contrast. The advantages of phase imaging are a significant decrease in radiation-induced damage and the ability to observe details of small objects for which absorption contrast is negligible.

In recent years, the focus of this research has been to develop accurate and rapid numerical methods of phase retrieval [1]. A number of approaches have been developed to achieve this aim, with the common requirement that intensity images are collected at a range of positions [2]. These images contain information on the redistribution of intensity as a function of propagation, which is related to the refractive index profile of the object.

Prior work on x-ray phase tomography has used phase contrast resulting from propagation to create 3-D phase visualization. In this technique, a sample is placed in a collimated x-ray beam, and the intensity distribution is measured some distance downstream. The refraction of the x-rays by phase gradients in the sample produces an intensity modulation at the detector plane and so allows a form of phase visualization. For a pure phase object, the measured intensity describes the Laplacian of the 2-D projection of the real part of the 3-D refractive index distribution. The tomographic reconstruction would therefore describe the 3-D Laplacian of the real part of the refractive index.

In 2-D x-ray microscopy, phase information can yield compositional information if the sample thickness is known. Conversely, the thickness may be determined if the composition is known. However, if fully 3-D phase and amplitude tomographic techniques are possible, *a priori* information is unnecessary for the reconstruction of a 3-D map of the full complex refractive index. This work

demonstrates such an approach with submicrometer spatial resolution.

## Methods and Materials

In the case of soft x-rays, we have recently [3] demonstrated accurate nanometer-scale quantitative phase 2-D imaging with the imaging microscope shown in Fig. 1. We used the same arrangement for this tomographic study at the SRI-CAT beamline 2-ID-B at APS.

A monochromatic (1.83 keV) beam of soft x-rays was defined by a 20- $\mu\text{m}$ -diameter aperture in order to provide a highly coherent source of illumination for the x-ray microscope. This beam passed through the sample; in this case, a commercially available atomic force microscope (AFM) tip. The zone plate created a first-order real image of the sample, 977 mm from the zone plate. In this arrangement, the object was magnified approximately 160 times. In our previous work [3], we demonstrated that this setup provides an imaging resolution of approximately 150 nm, limited by the camera pixel size.

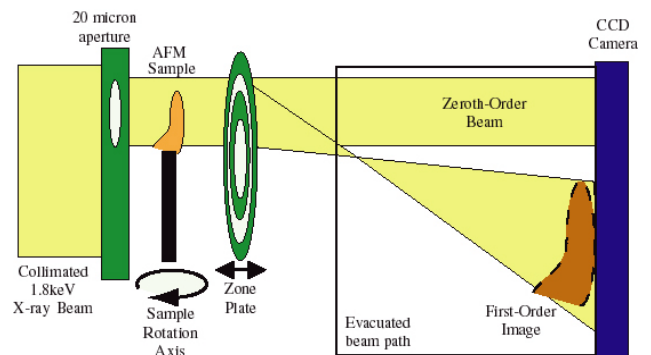


FIG. 1. Schematic of soft x-ray imaging microscope used in this work.

## Results

Figure 2a shows a background-corrected image of the AFM tip obtained with this system. Note that the image contrast is very poor, as would be expected for an in-focus image of a sample that has very little absorption. The total height of these AFM images is approximately 9  $\mu\text{m}$ , and the tip base is approximately 6.8  $\mu\text{m}$  across.

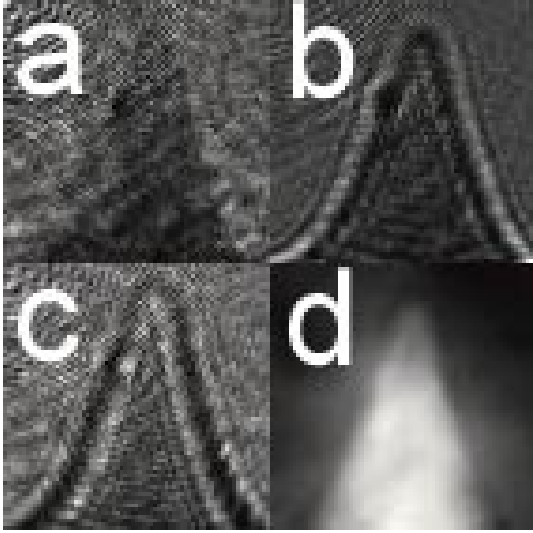


FIG. 2. Examples of typical 2-D image data for the AFM tip sample. (a) Typical “in-focus” absorption image of the AFM tip corrected for the sample free field. (b) 1-mm overfocus. (c) 1-mm underfocus phase contrast images of the AFM tip corrected for the sample free field. (d) 2-D phase projection recovered by applying the phase recovery method to the intensity data shown.

In order to estimate the intensity derivative, two defocused images were recorded on either side of the in-focus position. A defocus distance of 1 mm on either side of the in-focus position was used, where the defocus was achieved by using a linear translation of the zone plate along the optical axis. Examples of typical “overfocus” and “underfocus” images corrected for the sample free field are shown in Figs. 2b and 2c, respectively.

After alignment and preprocessing of the projection data, such as cropping and equilibration to compensate for variations in the beam intensity, a 2-D projected phase map may be obtained. A typical example is shown in Fig. 2d, where the dramatically improved contrast with phase imaging is clearly evident. This process was repeated at angular intervals of  $1^\circ$  over a range of  $180^\circ$ . Note that in order to ensure that a strong phase signature was obtained, the defocus distance was larger than is optimal for recovery of high spatial resolution in the phase image. By suitable alignment of individual projections, we obtained sufficient intensity and phase projections to allow tomographic reconstruction.

By using the techniques described, phase data similar to those in Fig. 2d were obtained for each projection and reconstructed into a 3-D image by using the filtered back projection method. Examples of the resulting *quantitative* 3-D phase reconstructions are shown in Fig. 3. These data

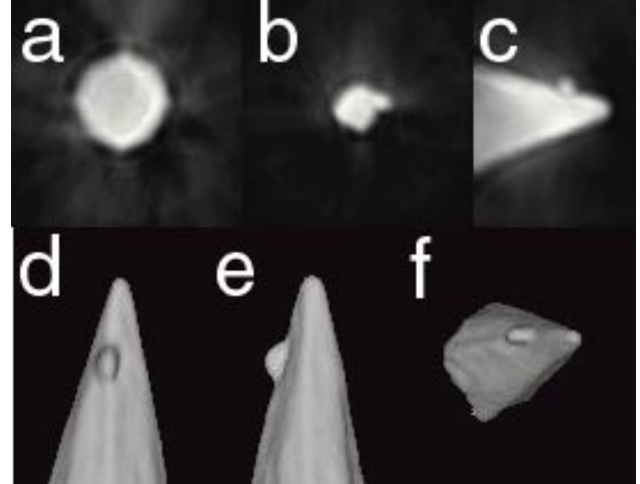


FIG. 3. *Quantitative tomographic reconstructions of 3-D maps of the real part of the refractive index.* (a) Horizontal slice of AFM tip. (b) Second slice including the  $900\text{-nm}^3$  spherical bump. (c) Vertical slice through the tomographic phase data. (d–f) Volume renderings of the real component of the refractive index of the AFM tip. The total height of this tip is  $9\ \mu\text{m}$ , and the average width is  $6.8\ \mu\text{m}$ .

represent measurements of the real part of the refractive index, as a function of position within the tip. Figs. 3a and 3b represent slices through the tip in the horizontal direction, whereas Fig. 3c depicts a slice of the reconstruction through the vertical direction.

## Discussion

Careful measurements from this reconstruction indicate that object details with a characteristic length of 900 nm are clearly resolved. This claim is supported by the 900-nm (6-pixel) diameter of the spherical bump visible in Figs. 3b and 3d, which we attribute to a defect in the AFM tip. Also notice the faceted nature apparent in Figs. 3a and 3b, which is typical of the manufacturing process used to etch crystalline AFM tips. Figures 3d-3f show volume renderings of the real part of the refractive index for the AFM tip. Here, the facet structure and spherical bump are clearly visible.

The analysis of the reconstructed phase volume data obtained provides a measured value of the refractive index decrement of  $\delta = (5.0 \pm 0.5) \times 10^{-5}$ . Theoretical calculations based on the known composition of the AFM tip suggest a figure of  $\delta = 5.06 \times 10^{-5}$  at this energy. The agreement is well within experimental error and confirms that it is possible to obtain a high-resolution quantitative map of the real part of the refractive index.

## **Acknowledgments**

This work was supported by the Australian Synchrotron Research Program, which is funded by the Commonwealth of Australia under the Major National Research Facilities Program, by the Australian Research Council. Use of the APS was supported by the U.S. Department of Energy, Office of Science, Office of Basic Energy Sciences, under Contract No. W-31-109-ENG-38.

## **References**

- [1] D. Paganin and K. A. Nugent, *Phys. Rev. Lett.* **80**, 2586-2589 (1998).
- [2] P. Cloetens, W. Ludwig, J. Baruchel, D. Van Dyck, J. Van Landuyt, J. P. Guigay, and M. Schlenker, *Appl. Phys. Lett.* **75**, 2912-2914 (1999).
- [3] B. E. Allman, P. J. McMahon, J. B. Tiller, K. A. Nugent, D. Paganin, A. Barty, L. McNulty, S. P. Frigo, X. Wang, and C. C. Retsch, *J. Opt. Soc. Am. A* **17**, 1732 (2000).